Integral Equation Theory of Polymer Solutions: Application to Polyethylene/Benzene Solutions

Sergio Mendez

University of New Mexico, Albuquerque, New Mexico 87131

John G. Curro*

Sandia National Laboratories, Albuquerque, New Mexico 87185

Received October 9, 2003; Revised Manuscript Received January 8, 2004

ABSTRACT: Solutions of polyethylene macromolecules immersed in benzene were modeled with self-consistent polymer reference interaction site model (PRISM) theory. The PRISM integral equations for the solution were solved self-consistently for the polyethylene intramolecular chain structure and intermolecular polymer and solvent correlations at various mole fractions. We found that explicitly considering the solvent molecules leads to considerably more short-range structure in the radial distribution function of the polymer, relative to the polymer without solvent at the same concentration. The long-range intermolecular correlations between polymer sites in the correlation hole regime decreased inversely with the polymer concentration as expected. The solvent/solvent radial distribution function, however, showed unexpected changes in shape and intensity as the polymer concentration increased. By using the direct correlation functions from PRISM theory, along with the random phase approximation, we estimated the spinodal temperatures as a function of polymer concentration. PRISM theory, which includes compressibility and nonrandom mixing effects, predicted a significantly higher critical temperature than was obtained from the corresponding incompressible Flory−Huggins theory. The PRISM spinodal curves were in reasonable agreement with experimental dissolution temperatures for octacosane in benzene.

I. Introduction

Most treatments of polymer solutions by theory and simulation do not explicitly account for the packing of the solvent molecules. Instead, the polymer is usually regarded as being in a "continuum" or vacuum solvent where the solvent molecules are either ignored, or replaced by a solvation potential. In most applications of self-consistent field theory, the field is local and does not account for the nonzero size of actual solvent molecules. The motivation for the present work is to elucidate the effect of modeling polymer solutions with explicit solvent molecules on the polymer structure. We employ the *polymer reference interaction site model* or PRISM theory[1] for this purpose.

Using computer simulation methods to model polymer solutions with explicit solvent molecules requires extensive computational resources. This is especially true when treating dilute polymer solutions due to the substantial time required to move the many solvent molecules, and due to the large simulation cell needed to ensure proper statistics. Nonetheless, recent work has been reported on coarse-grained[2−5] and atomistic[6,7] simulations of dilute polymer solutions.

PRISM theory was employed by Khalatur et al.[8,9] to study polymers in infinitely dilute solutions. Other theoretical methods were also directed at the dilute solution problem.[10,11] Recently, Mendez et al.[5] reported on the use of PRISM theory to model an athermal solution of tangent site polymer chains immersed in a spherical monatomic solvent over a wide range of concentration and chain lengths. By solving PRISM theory self-consistently for the intramolecular structure, they computed[5] scaling exponents in accordance with expected results for a chain in dilute solution and in a melt. Interestingly, Mendez et al. also observed that the presence of explicit solvent molecules led to short-range structural features in the intermolecular pair correlation function $g_{pp}(r)$ of the polymer that were not present with a vacuum solvent at the same polymer concentration. In this previous PRISM study, the monomer and solvent sizes were identical hence there was only a single local length scale. The purpose of this investigation was to see if similar short-range features in $g_{pp}(r)$ are present with a real polymer in a real solvent where multiple length scales are present. For this purpose, we chose to study polyethylene in a benzene solvent.

II. Theory and Computation

A. PRISM Theory. Curro and Schweizer[1,12−14] developed PRISM theory from an extension to polymers of Chandler and Andersen's[15,16] *reference interaction site model*, or RISM, theory. In both theories, all molecules are modeled as overlapping, spherically symmetric interaction sites. In the case of polyethylene (PE), the chains are assumed to consist of $N_p = N$ equivalent sites corresponding to CH_2 groups where end effects are ignored. Lowden and Chandler[17] first applied RISM theory to liquid benzene that they modeled as six equivalent, overlapping hard sites representing aromatic CH groups. Thus, the PE/benzene solution only requires two independent sites to characterize the molecular packing.

The output of self-consistent PRISM theory is the intramolecular structure of the polymer chains, and the intermolecular radial distribution functions between polymer/polymer, $g_{pp}(r)$, polymer/solvent, $g_{sp}(r)$, and solvent/solvent, $g_{ss}(r)$, sites. The generalized Ornstein−Zernike equation[1,12−16] (shown below in Fourier transform space) serves to define the corresponding direct correlation functions ($C_{pp}(r)$, $C_{sp}(r)$, $C_{ss}(r)$),

10.1021/ma0355296 CCC: $27.50 © 2004 American Chemical Society
Published on Web 02/13/2004

$$\hat{\mathbf{H}}(k) = \hat{\Omega}(k)\cdot\hat{\mathbf{C}}(k)\cdot[\hat{\Omega}(k) + \hat{\mathbf{H}}(k)] \quad (1)$$

where in real space, the matrix $H_{\alpha\gamma}(r)$ is defined as

$$H_{\alpha\gamma}(r) = \rho_\alpha \rho_\gamma [g_{\alpha\gamma}(r) - 1] \quad (2)$$

The α and γ denote s or p, and ρ_α is the density of sites of type α. The intramolecular structure factor can be expressed as

$$\hat{\Omega}_{\alpha\gamma}(k) = \frac{\delta_{\alpha\gamma}}{N_\alpha}\sum_{i\in\alpha}\sum_{j\in\gamma}\left\langle\frac{\sin kr_{ij}}{kr_{ij}}\right\rangle \quad (3)$$

where the summation is taken over all sites on a chain with N_p monomers or the solvent of N_s sites. For a rigid benzene molecule, the intramolecular structure factor, $\hat{\Omega}_{ss}(k)$, can be calculated exactly[17] from the geometry of a benzene ring using eq 3.

$$\hat{\Omega}_{ss}(k) = 1 + 2\frac{\sin(kl)}{kl} + 2\frac{\sin(\sqrt{3}kl)}{\sqrt{3}kl} + \frac{\sin(2kl)}{kl} \quad (4)$$

where l is the bond length between CH groups. In our treatment of flexible PE chains, the intramolecular structure, $\hat{\Omega}_{pp}(k)$, is determined by a single-chain MC simulation. In this simulation, the sites are affected by both a repulsive Lennard-Jones interaction and by a solvation potential (to be discussed later).

For a given $\hat{\Omega}_{\alpha\gamma}(k)$ matrix, we use eq 1, together with a closure approximation, to solve for both $\hat{H}_{\alpha\gamma}(k)$ and $\hat{C}_{\alpha\gamma}(k)$. For this purpose, we employ the atomic Percus−Yevick (PY) approximation[1,18] for the direct correlation function

$$C_{\alpha\gamma}(r) = \{1 - \exp[\beta u^{rep}_{\alpha\gamma}(r)]\}\,[H_{\alpha\gamma}(r) + 1] \quad (5)$$

Here $\beta = 1/k_BT$ and $u^{rep}_{\alpha\gamma}(r)$ is a repulsive, reference interaction potential. We used the atomic PY approximation because it is accurate[1] in describing liquids with strong repulsions and weak attractions of the type we expect in polyethylene/benzene solutions. However, we only use the repulsive part of the potential because it has been demonstrated previously[1] that the atomic closures, when used with PRISM theory, overestimate the effect of attractions on concentration fluctuations in polymer mixtures. The molecular closures[19,20] of Yethiraj and Schweizer have been demonstrated to overcome this problem. However, the molecular closures are formulated for a hard core potential with an attractive tail. Since in this work we are using continuous site/site potentials, the molecular closures would not be applicable.

The repulsive, or reference, interaction is defined by a decomposition of the full LJ 6−12 potential as proposed by Weeks, Chandler, and Andersen (WCA),[21]

$$u^{rep}_{\alpha\gamma}(r) = 4\epsilon_{\alpha\gamma}\left[\left(\frac{\sigma_{\alpha\gamma}}{r}\right)^{12} - \left(\frac{\sigma_{\alpha\gamma}}{r}\right)^{6} + \frac{1}{4}\right], \quad r \le \sigma_{\alpha\gamma}2^{1/6}$$

$$u^{rep}_{\alpha\gamma}(r) = 0, \quad r > \sigma_{\alpha\gamma}2^{1/6} \quad (6a)$$

and the attractive, or perturbative, portion is

$$u^{att}_{\alpha\gamma}(r) = -\epsilon^{att}_{\alpha\gamma}, \quad r < \sigma_{\alpha\gamma}2^{1/6}$$

$$u^{att}_{\alpha\gamma}(r) = 4\epsilon^{att}_{\alpha\gamma}\left[\left(\frac{\sigma_{\alpha\gamma}}{r}\right)^{12} - \left(\frac{\sigma_{\alpha\gamma}}{r}\right)^{6}\right], \quad r \ge \sigma_{\alpha\gamma}2^{1/6} \quad (6b)$$

where $\epsilon_{\alpha\gamma}$ and $\sigma_{\alpha\gamma}$ are the usual LJ parameters. The PRISM calculations are performed with the reference potential, $u^{rep}_{\alpha\gamma}(r)$. Since it is well-known that the packing in dense liquids is determined almost entirely by the repulsive branch of the potential,[18] we expect the PY closure to yield accurate pair correlation functions of the polymer solution. The structural information from these calculations can then be used along with the "turned on" attractive potential to estimate the spinodal temperature. The TrAPPE-UA force field for hydrocarbons of Martin and Siepmann[22] has been used to model the PE molecules.

We utilize an iterative scheme to self-consistently solve for the intra- and intermolecular structure of the PE chains in solution. At the heart of this scheme is the determination of the solvation potential $W_{\alpha\gamma}(r)$ which, for the polymer/polymer component, is attractive at small values of r. Assuming pairwise additivity, $\hat{W}_{pp}(k)$ (in Fourier transform space) can be approximately calculated[1,23,24] from

$$\beta\hat{W}_{pp}(k) \cong -K\sum_{i,j}\hat{C}_{pi}(k)\hat{S}_{ij}(k)\hat{C}_{jp}(k) \quad (7)$$

where the structure factors are defined according to

$$\hat{S}_{\alpha\gamma}(k) = \rho_\alpha\hat{\Omega}_{\alpha\gamma}(k) + \hat{H}_{\alpha\gamma}(k) \quad (8)$$

We introduce a constant K close to unity in eq 7 that can be used to tune the solvation potential to reproduce the radius of gyration of the polymer (if known). To begin our iterative scheme, we first guess the solvation potential and use this in a single-chain Monte Carlo simulation[25] to calculate $\hat{\Omega}_{pp}(k)$. With $\hat{\Omega}_{pp}(k)$, we use eqs 1 and 5 to solve for $\hat{H}_{\alpha\gamma}(k)$ and $\hat{C}_{\alpha\gamma}(k)$. This then allows us to calculate a new solvation potential with eq 7, and we continue to iterate until the difference between the new and old solvation potentials becomes very small. It should be mentioned that it is not necessary to perform a new Monte Carlo simulation with each iteration. Reweighting techniques[25] can be used to greatly reduce the number of simulations that need to be carried out during the course of the self-consistent calculation. The final output of PRISM theory gives a self-consistent solution of the intra, $\hat{\Omega}_{pp}(k)$, and intermolecular, $g_{\alpha\gamma}(r)$, structure.

B. Spinodal Temperature. To approximate the phase behavior of a polymer solution, we used the structural information contained in the direct correlation functions that were obtained from PRISM calculations using the reference LJ potential. An exact expression for the spinodal condition of a compressible, binary system was derived by Curro and Schweizer[26]

$$1 - \rho_p N_p \hat{C}_{pp}(0) - \rho_s N_s \hat{C}_{ss}(0) + \rho_p N_p \rho_s N_s [\hat{C}_{pp}(0)\hat{C}_{ss}(0) - \hat{C}_{sp}{}^2(0)] = 0 \quad (9)$$

To estimate the spinodal temperature it is necessary to account for the attractive branch of the potential. Hence, we invoked the random phase approximation (RPA)[18] as a means to relate the direct correlation functions to the attractive potentials (and thus "turn

Table 1. Summary of Lennard-Jones Parameters from Three Models of Benzene

authors	technique	σ (Å)	ϵ/k_B (K)	B (Å)	ρ (g/cm^3)
EW[30]	MC	3.5	77.0	1.756	0.859
CFR[31]	MD	3.72	55.3	1.410	0.874
WMS[32]	MC	3.695	50.5	1.40	

on" the attractions),

$$\hat{C}_{pp}(0) \cong \hat{C}^{o}_{pp} - \beta\hat{u}^{att}_{pp}(0)$$
$$\hat{C}_{ss}(0) \cong \hat{C}^{o}_{ss} - \beta\hat{u}^{att}_{ss}(0)$$
$$\hat{C}_{sp}(0) \cong \hat{C}^{o}_{sp} - \beta\hat{u}^{att}_{sp}(0) \qquad (10)$$

$\hat{C}^{o}_{\alpha\gamma}$ can be determined by extrapolating to zero wave vector the $\hat{C}_{\alpha\gamma}(k)$ of the reference system. The Fourier transform of the attractive potential, $\hat{u}^{att}_{\alpha\gamma}(k)$, can be found analytically at zero wave vector.

$$\hat{u}^{att}_{\alpha\gamma}(0) = \frac{-64\pi\epsilon^{att}_{\alpha\gamma}\sigma_{\alpha\gamma}{}^3}{9\sqrt{2}} \qquad (11)$$

After substitutions and algebraic manipulation of eqs 9−11, the spinodal temperature, T_s, can be written as

$$T_S = \frac{64\pi}{k_B 9\sqrt{2}} \times \frac{\rho_s N_s \epsilon_{ss}\sigma_s{}^3(1 - \rho_p N_p \hat{C}^{o}_{pp}) + \rho_p N_p \epsilon_{pp}\sigma_p{}^3(1 - \rho_s N_s \hat{C}^{o}_{ss}) + 2\rho_s N_s \rho_p N_p \epsilon_{sp}\sigma_{sp}{}^3 \hat{C}^{o}_{sp}}{1 - \rho_s N_s \hat{C}^{o}_{ss} - \rho_p N_p \hat{C}^{o}_{pp} + \rho_s N_s \rho_p N_p (\hat{C}^{o}_{ss}\,\hat{C}^{o}_{pp} - \hat{C}^{o}_{sp}{}^2)} \qquad (12)$$

Assuming zero volume change on mixing, we can write,

$$\frac{1}{\rho} = \frac{\phi}{\rho^{o}_p} + \frac{(1-\phi)}{\rho^{o}_s}$$
$$\rho_p = \phi\rho, \quad \rho_s = (1-\phi)\rho \qquad (13a)$$

where ϕ is the polymer site fraction and, ρ^{o}_p, ρ^{o}_s, and ρ are the pure polymer, pure solvent and solution total densities, respectively. As noted above, T_s is related to the direct correlation functions from the reference system and the polymer and solvent densities; however, the temperature dependence of these densities can be expressed as

$$\rho^{o}_i(T) = \rho^{o}_i(T_o)[1 + \alpha_i(T - T_o)] \qquad (13b)$$

where α_i is the volume expansivity of species i (α_p = 0.00085 °C^{-1},[27] α_s = −0.00136 °C^{-1} [28]), and T_o is an arbitrary reference temperature (298 K). A numerical algorithm was used to find the spinodal temperature from eqs 12−13a,b.

III. Results and Discussion

In the Lowden and Chandler[17] model of benzene the CH sites were taken as overlapping hard spheres. Good agreement was found with wide-angle X-ray scattering measurements of Narten.[29] Subsequently, Evans and Watts[30] (EW), Claessens, Ferrario, and Ryackaert[31] (CFR), and Wick, Martin, and Siepmann[32] (WMS) proposed Lennard-Jones potentials for benzene. The LJ parameters and bond lengths obtained from these three studies are summarized in Table 1. It is important to note that all three groups performed simulations using full LJ potentials (with attractions and repulsions) whereas in our RISM calculations we only used repulsive LJ interactions. It should also be mentioned that electrostatic interactions, thought to be important for benzene, are not included in any of the three benzene potentials used in this work.

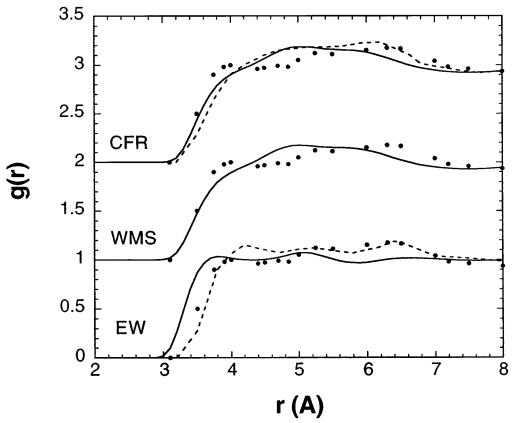

Figure 1. Intermolecular radial distribution function, $g(r)$, for pure liquid benzene. The points are from experiment,[29] the dashed lines are from either MC simulations (EW)[30] or from MD simulations (CFR),[31] and the solid lines are from RISM theory calculations. Some of the curves have been shifted along the vertical axis for clarity.

In Figure 1 are shown three sets of intermolecular radial distribution functions, $g(r)$, for pure liquid benzene using the three benzene Lennard-Jones potentials. In these plots, RISM theory is compared with results from both simulation and experimental data.[29] Qualitatively, the intermolecular $g(r)$'s are similar to the Lowden and Chandler results,[17] but as expected, the cusps that arise from the hard core nature of the potential are smoothed out when the continuous site/site potentials are used. On the basis of the center of mass distribution between molecules, Lowden and Chandler concluded that the benzene molecules tend to pack in a perpendicular fashion as suggested by Narten.[29] From Figure 1, it can be observed that there is reasonably good agreement between RISM theory and simulation. It can also be seen from this figure that the radial distribution functions from the CFR and WMS potentials fail to capture the finer structural features measured experimentally for liquid benzene. Although not strictly quantitative, the EW potential does exhibit these features.

We then solved the PRISM theory self-consistently for the polymer solution through the procedure described above. We varied the strength of the solvation potential K in eq 7 until the Flory exponent ν ($\langle R_e{}^2\rangle \propto N^{2\nu}$) of the pure polymer melt was close to its expected value. A log−log plot of the mean square end-to-end distance, $\langle R_e{}^2\rangle$, vs the number of monomers, N_p, is shown in Figure 2 for an infinitely dilute solution and the polymer melt for K = 1.047. The WMS potential was used in this case for benzene and the temperature was set to 350 K. Since the PRISM calculations only used the repulsive part of the potential, it is expected that the temperature will always be above the theta temperature. A power law fit of this plot yields a Flory exponent, ν, of 0.585 ± 0.03, close to the expected $^3/_5$ for a chain in a good solvent where excluded volume interactions are strong. Also shown in this figure is a similar plot for a polymer melt with a Flory exponent of 0.495 ± 0.03, in good agreement with the value of $^1/_2$

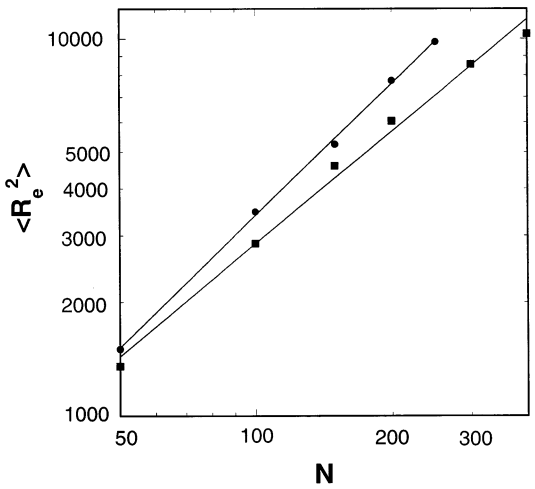

Figure 2. PRISM prediction for $\langle R_e^2 \rangle$ vs N of an infinitely dilute polyethylene/benzene solution at 350 K (circles). PRISM prediction of $\langle R_e^2 \rangle$ vs N for a polyethylene melt (squares) at 350 K. The straight lines are power-law fits of the PRISM results. The WMS model of benzene was used, and K in eq 7 was set to 1.047.

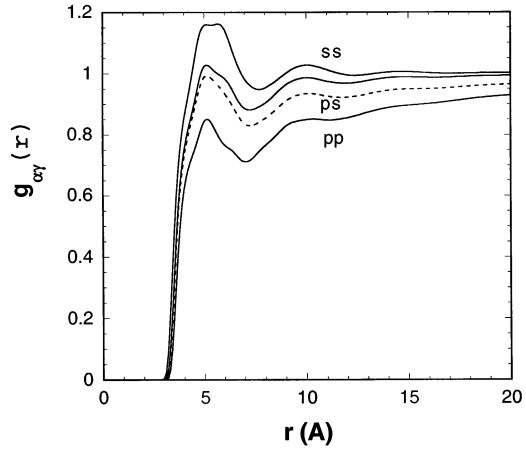

Figure 3. PRISM predictions (solid curves) for the radial distribution functions of a polymer solution at polymer site fraction $\phi = 0.10$ and 350 K. The dashed curve is an estimate for the cross term $g_{ps}(r) \cong \sqrt{g_{pp}(r)g_{ss}(r)}$. The WMS model of benzene was used and K in eq 7 was set to 1.047.

expected for a polymer melt where the excluded volume interactions are screened.

In Figure 3, we show the three intermolecular radial distribution functions between benzene CH sites, $g_{ss}(r)$, polyethylene CH_2 sites, $g_{pp}(r)$, and the cross term between solvent and polymer sites, $g_{sp}(r)$ for a solution of $\phi = 0.10$. Note the similarity in the short-range structure of benzene and polyethylene with a slight shoulder near ~4 Å and a prominent peak located at $r \sim 5$ Å in all three correlation functions. The shoulder in $g_{\alpha\gamma}(r)$ corresponds to a pair of sites near contact. The first peak in the $g_{\alpha\gamma}(r)$'s corresponds to a preferred distance between a pair of sites on different molecules, both in contact with an intermediate, covalently bonded site. Note that the benzene correlation function is broader than the corresponding $g(r)$ for polyethylene in the 5 Å range for the WMS benzene potential. In fact this broad peak actually consists of two overlapping peaks at ~5 and 5.8 Å. Whereas the 5 Å feature corresponds to a pair of intermolecular benzene CH sites in contact with one intermediate site, the 5.8 Å peak probably involves two intermediate sites. The $g_{pp}(r)$

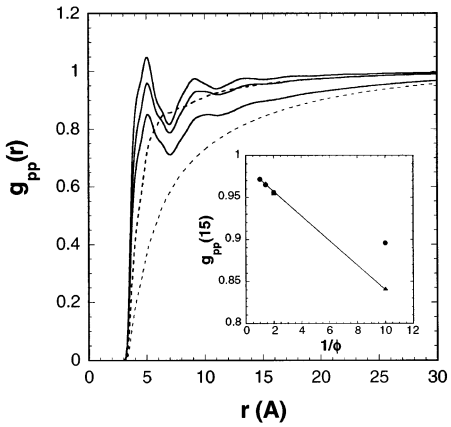

Figure 4. Polymer/polymer radial distribution function $g_{pp}(r)$ ($N = 100$, $T = 350$ K) at various site fractions of polymer $\phi = 1.0$ (upper solid), 0.50 (middle solid), 0.10 (lower solid) with explicit solvent present. The dashed curves refer to $g_{pp}(r)$ at $\phi = 0.50$ (upper) and 0.10 (lower) when the solvent molecules are removed. The inset depicts $g_{pp}(15)$ in the correlation hole regime as a function of $1/\phi$ for the explicit solvent (circles) and vacuum solvent (triangles) cases. The line is a fit to the data as suggested by eq 18. The WMS model of benzene was used, and K in eq 7 was set to 1.047.

between polymer CH_2 sites consists of the short-range local structure superimposed on a correlation hole where $g_{pp}(r) \to 1$ on a scale corresponding to the radius of gyration. The cross term can be seen to deviate significantly from a random mixing estimate $g_{ps}(r) \cong \sqrt{g_{pp}(r)g_{ss}(r)}$ shown as the dashed curve.

In several previous investigations[33−35] PRISM theory was used to calculate the structure of pure PE melts. Our muticomponent PRISM calculations, presented here for polyethylene solutions, reproduce the melt structure in the zero solvent concentration limit. In Figure 4, we display $g_{pp}(r)$ for polymer solutions ($N_p = 100$) over a range of concentrations. Also shown in this plot are the polymer/polymer pair correlation functions at the same concentrations (densities) for the vacuum solvent case when no solvent molecules are present.

It can be seen from Figure 4 that $g_{pp}(r)$ has considerably more short-range structure in the explicit solvent than in the vacuum solvent. This is consistent with what was observed in our earlier study[5] of tangent-site polymer solutions. The fact that the polymer packing is different in the explicit and vacuum solvents is not surprising when one considers the equations that govern $g_{pp}(r)$. From the generalized Ornstein−Zernike equation in eq 1 we can write that $h_{pp}(r) = g_{pp}(r) - 1$ is given by

$$\hat{h}_{pp}(k) = \frac{\hat{\Omega}_{pp}{}^2(k)[\hat{C}_{pp}(k) - \rho_s\hat{\Omega}_{ss}(k)(\hat{C}_{pp}\hat{C}_{ss} - \hat{C}_{sp}{}^2)]}{1 - \rho_p\hat{\Omega}_{pp}(k)\hat{C}_{pp}(k) - \rho_s\hat{\Omega}_{ss}(k)\hat{C}_{ss}(k) + \rho_s\rho_p\hat{\Omega}_{ss}\hat{\Omega}_{pp}(\hat{C}_{pp}\hat{C}_{ss} - \hat{C}_{sp}{}^2)} \quad (14)$$

for the packing of polymers in an explicit solvent. Thus, it can be seen that presence of the solvent affects the polymer packing through terms involving ρ_s, $\hat{\Omega}_{ss}$, $\hat{C}_{ss}$ and $\hat{C}_{sp}$. By contrast, in the vacuum solvent we have a one-component system at density ρ_p and the polymer packing reduces to

$$\hat{h}^0_{pp}(k) = \frac{\hat{\Omega}_{pp}{}^2(k)\hat{C}^0_{pp}(k)}{1 - \rho_p\hat{\Omega}_{pp}(k)\hat{C}^0_{pp}(k)} \quad (15)$$

where the superscript denotes the vacuum solvent situation. In eq 15, the solvent plays no role other than to lower the density of the system. One consequence of the differences in eqs 14 and 15 is that the compressibility of the polymer in a vacuum solvent is very high at low polymer density, whereas the compressibility in the explicit solvent solution remains liquidlike at all concentrations. It should be mentioned that for the low-density calculations in the absence of solvent, the packing of the polymer may be influenced by the neglect of attractive interactions to a greater extent than for the dense systems with solvent present. However, the qualitative comparisons between polymer solutions with and without explicit solvent should not change.

On long length scales it can be observed from Figure 4 that $g_{pp}(r)$ is similar for the polymer in explicit and vacuum solvents. In fact at the higher concentrations of $\phi = 0.50$ and 0.70 (not shown) $g_{pp}(r)$ in the correlation hole regime are in close agreement for both solvents. At the lowest concentration of $\phi = 0.10$, the correlation hole of the vacuum solution is larger than for the explicit solvent. The radial distribution of a polymer system on long length scales can be approximated[1] by a *thread model* for which the diameter d of the monomer shrinks to zero and $\rho_p \rightarrow \infty$ such that the reduced density $\rho_p d^3$ remains finite. The hard core condition in this limit reduces to $g_{pp}(0) = 0$. With these simplifications, the PRISM theory for the thread model liquid can be solved analytically to give[1]

$$g_{pp}(r) = 1 + \frac{3}{\pi\rho_p\sigma^2 r}[\exp(-r/\xi_p) - \exp(-\sqrt{2}r/R_g)] \quad (16)$$

where the local polymer screening length is defined as

$$\frac{1}{\xi_p} = \frac{\pi\rho_p\sigma^2}{3} + \frac{\sqrt{2}}{R_g} \quad (17)$$

On long length scales in the correlation hole regime where $r \gg \xi_p$, $g_{pp}(r)$ approaches unity in a Yukawa fashion

$$g_{pp}(r) \sim 1 - \frac{3}{\pi\rho_p\sigma^2 r}\exp(-\sqrt{2}r/R_g) \quad (18)$$

This behavior is seen in both the explicit and vacuum solvents in the correlation hole regime where the radius of gyration R_g is the relevant length scale. At low polymer concentrations, we find that the chain dimensions are higher in the vacuum solvent relative to polymer in the explicit solvent. In this respect, the vacuum solvent is a *better solvent* than the explicit solvent in dilute solution. Thus, the range of the correlation hole will be larger in the vacuum solvent case at low concentrations.

We now examine the concentration dependence of the polymer radial distribution function. From Figure 4 it can be observed that in the explicit solvent, the short-range structure of $g_{pp}(r)$ retains the same shape but each curve is systematically lowered as the concentration of polymer is reduced. This is indeed what one would expect based on the thread model structure in eq 16. For large $r \gg \xi_p$ eq 18 predicts that $h_{pp}(r) \propto 1/\rho_p$. This trend is seen for both the explicit and vacuum solvent cases in the inset of Figure 4 where $g_{pp}(15)$ is plotted vs $1/\phi$. Linear behavior is seen at the higher concentrations; at the lowest concentration ($\phi = 0.10$) the condition $r \gg \xi_p$ is not satisfied and additional concentration dependence enters through ξ_p in eq 17.

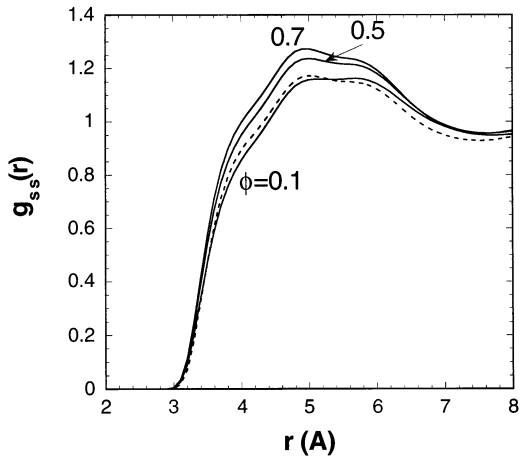

Figure 5. Solvent/solvent radial distribution function $g_{ss}(r)$ ($N = 100$, $T = 350$ K) at various fractions of polymer ϕ (solid curves) as indicated in the figure. The dashed curve corresponds to the pure benzene liquid. The WMS model of benzene was used, and K in eq 7 was set to 1.047.

It is interesting to study the packing of the benzene molecules as the concentration of polyethylene is increased. Figure 5 depicts $g_{ss}(r)$ for the pure solvent and the various polymer solutions. Our expectation was that the structural features in the solvent radial distribution function would stay the same or systematically decrease as polymer is added to the solution, and the average distance between benzene molecules becomes larger. The opposite trend is seen in Figure 5. As polymer is initially added to the pure benzene liquid, the shoulder near contact at ~3.8 Å and the peak near 5 Å slightly drop, whereas the peak near 5.8 Å increases as seen at $\phi = 0.10$. As still more polymer is added, all the features in the range $3.8 \leq r \leq 5.8$ surprisingly increase as the polymer concentration increases from $\phi = 0.10$ to 0.70. One possible explanation for this surprising behavior is that polyethylene chains tend to disrupt the preferred perpendicular packing[17,29] of benzene molecules thought to exist in the pure solvent. In solution the correlations between solvent sites are now mediated by sites on the polymer chains. This can be seen in Figure 6 where the polymer/solvent radial distribution function near contact (~3.5−4 Å) continues to increase as the polymer concentration increases. In order for benzene molecules to occupy the space between polymer sites, it is not unreasonable to expect the orientation between benzene rings to become more random.

We now present results for the spinodal curve of PE/benzene solutions using the estimate provided by invoking the RPA approximation in eqs 12, together with the assumption of zero volume change of mixing in eqs 13a and 13b. In Figure 7, we plotted the PRISM/RPA estimate of the spinodal temperature for the alkane octacosane ($C_{28}H_{58}$) solution using the WMS model for benzene. It is instructive to compare this with what one would predict from a continuum generalization of the Flory−Huggins theory. For an incompressible liquid, the three direct correlation functions have the same limit

$$\hat{C}^o_{pp}(k), \quad \hat{C}^o_{ss}(k), \quad \hat{C}^o_{sp}(k) \rightarrow -\infty \quad (19)$$

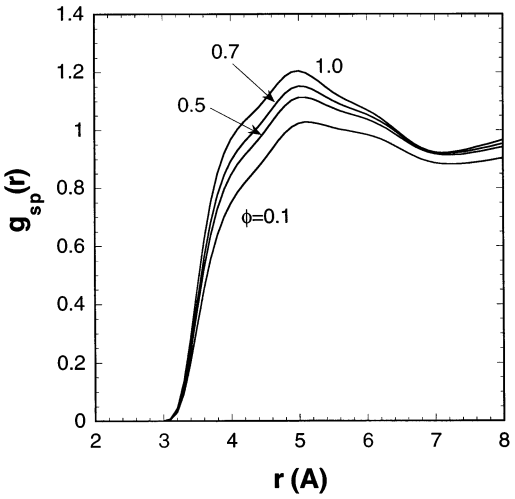

Figure 6. Cross radial distribution function $g_{sp}(r)$ ($N = 100$, $T = 350$ K) at various fractions of polymer ϕ as indicated in the figure. The WMS model of benzene was used, and K in eq 7 was set to 1.047.

Imposing this incompressibility limit on eq 12 results in

$$k_B T_S = \frac{(64\pi/9\sqrt{2})\rho_s\rho_p N_s N_p \left[\epsilon_{ss}\sigma_s^3\sqrt{\frac{\hat{C}^o_{pp}}{\hat{C}^o_{ss}}} + \epsilon_{pp}\sigma_p^3\sqrt{\frac{\hat{C}^o_{ss}}{\hat{C}^o_{pp}}} - 2\epsilon_{ss}\sigma_{sp}^3\frac{\hat{C}^o_{sp}}{\sqrt{\hat{C}^o_{ss}\hat{C}^o_{pp}}}\right]}{\rho_s N_s\sqrt{\frac{\hat{C}^o_{ss}}{\hat{C}^o_{pp}}} + \rho_p N_p\sqrt{\frac{\hat{C}^o_{pp}}{\hat{C}^o_{ss}}}} \tag{20}$$

If the site volumes v_s and v_p of solvent and polymer are not equal, then the ratios of direct correlation functions in eq 20 are not unity in the incompressible limit as in our previous study.[5] We can proceed further by making use of the zero volume of mixing assumption. This condition implies that the partial molar site volumes $\bar{v}_p$ and $\bar{v}_s$ are equal to their respective site volumes. From the Kirkwood and Buff[36] relations for the partial molar volumes of a mixture, we can write

$$\frac{v_s}{v_p} = \frac{\rho_s\hat{C}^o_{ss} + \rho_p\hat{C}^o_{sp}}{\rho_s\hat{C}^o_{sp} + \rho_p\hat{C}^o_{pp}} \tag{21}$$

where we have made use of the fact that $\hat{S}^{-1}_{\alpha\gamma}(0) \rightarrow -\hat{C}^0_{\alpha\gamma}$ in the incompressible limit. For eq 21 to hold at all concentrations implies that

$$\hat{C}^o_{sp} = \sqrt{\hat{C}^o_{ss}\hat{C}^o_{pp}} \quad \text{and} \quad \frac{\hat{C}^o_{ss}}{\hat{C}^o_{pp}} = \frac{\sigma_{ss}^6}{\sigma_{pp}^6} \tag{22}$$

for an incompressible mixture with zero volume change of mixing. In writing eq 22 we have assumed that $R = v_s/v_p = \sigma_{ss}^3/\sigma_{pp}^3$. Substitution of eq 22 into eq 20 leads to the continuum analogue of the Flory−Huggins theory for the spinodal temperature.

$$k_B T_S = \frac{(64\pi/9\sqrt{2})(R^{-1}\epsilon_{ss}\sigma_{ss}^3 + R\epsilon_{pp}\sigma_{pp}^3 - 2\epsilon_{sp}\sigma_{sp}^3)}{R/\rho_p N_p + 1/R\rho_s N_s} \tag{23}$$

Equation 23 can be considered a generalization of the mean field Flory−Huggins theory to the case where the monomer and solvent sizes are different.[26] This Flory−Huggins prediction is plotted in Figure 7 as the dashed curve. Note that nonrandom mixing and compressibility effects in PRISM theory lead to an increase in the spinodal temperature and the tendency of the octacosane/benzene solution to demix. This is qualitatively similar to what we observed in our earlier study[5] of coarse-grained polymer solutions.

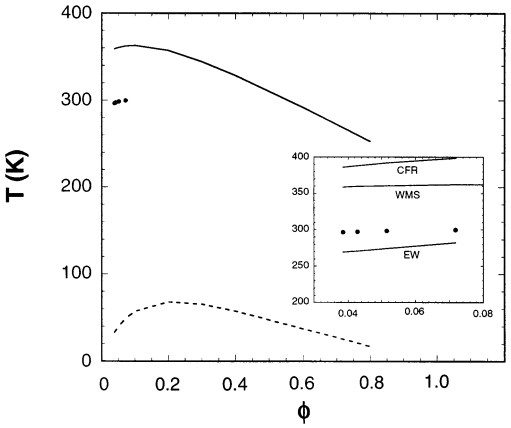

Figure 7. Approximate spinodal curve calculated with the PRISM/RPA approximation from eq 12 (solid curve) and with the incompressible Flory−Huggins expression from eq 23 (dashed curve). The points are experimental data of Haulait-Pirson, Huys, and Vanstraelen.[37] The WMS model of benzene was used and K in eq 7 was set to 1.047. The inset is a blowup of the spinodal curve in the region of the experimental data. The inset shows the PRISM/RPA results with the three models of benzene indicated in the figure.

Also shown in Figure 7 are the experimental points[37] from dissolution temperatures of octacosane in benzene. In the inset of Figure 7, we have expanded the scale of the plot in the region of the experimental data and show PRISM/RPA predictions for the three different models of benzene. Note the large sensitivity of the predictions to the benzene potential. In the present case the EW model[30] for the solvent gives the closest agreement with experiment. However, the RPA approximation in eq 12 should be viewed as a very approximate estimate of the actual spinodal.

IV. Conclusions

In this paper we have presented the results of self-consistent PRISM theory for the packing of macromolecules and solvent in the PE/benzene solution. The calculations clearly demonstrate that the size and shape of the solvent molecules affects the short- range packing of the polymer. $g_{pp}(r)$ shows considerably more short-range structure than the corresponding polymer in a vacuum. In contrast, the long range, correlation hole regime is similar both with and without explicit solvent molecules present and changes with concentration in a manner predicted from the analytical thread model.

The short-range correlation function $g_{ss}(r)$ of the benzene molecules unexpectedly changed with increasing polymer concentration. Of course this effect may be due to the approximate nature of the closure approximation and/or the solvation potential given in eqs 5 and 7. If the trend is indeed real, we speculate that it may be a signal that the perpendicular packing of the benzene rings, thought to occur in pure liquid benzene, is disrupted by the polyethylene chains in solution. This speculation could be investigated in more detail by performing center-of-mass RISM calculations on the

polyethylene/benzene solution of the type performed by Lowden and Chandler[17] on pure benzene with an auxiliary site at the center of the ring. The question of preferential orientation of the benzene rings could be addressed more definitively through computer simulations of alkane/benzene mixtures. In this case orientational correlations between benzene rings could be directly calculated as a function of concentration.

Our approximate RPA estimate of the spinodal curves for the PE/benzene solution suggests that nonrandom mixing and compressibility effects decrease the miscibility of the solution and raise the critical point relative to the incompressible mean field theory. More exact PRISM calculations, beyond the RPA estimate, are problematic because of the previously demonstrated[1] inaccuracy of the atomic PY closure to capture the subtle effects of attractions on the intermolecular packing in polymer blends.

Acknowledgment. Sandia is a multiprogram laboratory operated by Lockheed Martin Co. for the U.S. Department of Energy under Contract No. DE-AC04094AL85000. The authors would like to thank K. S. Schweizer and J. D. McCoy for helpful discussions.

References and Notes

(1) Schweizer, K. S.; Curro, J. G. *Adv. Chem. Phys.* **1997**, *98*, 1.
(2) Suen, J. K. C.; Escobedo, F. A.; de Pablo, J. J. *J. Chem. Phys.* **1997**, *106*, 1288.
(3) Luna Barcenas, G.; Gromov, D. G.; Meredith, J. C.; Sanchez, I. C.; de Pablo, J. J.; Johnston, K. P. *Chem. Phys. Lett.* **1997**, *278*, 302.
(4) Ahlrichs, P.; Dünweg, B. *J. Chem. Phys.* **1999**, *111*, 8225.
(5) Mendez, S.; Curro, J. G.; Pütz, M.; Bedrov, D.; Smith, G. D. *J. Chem. Phys.* **2001**, *115*, 5669.
(6) Smith, G. D.; Bedrov, D.; Borodin, O. *Phys. Rev. Lett.* **2000**, *85*, 5583.
(7) Smith, G. D.; Bedrov, D.; Bododin, O. *J. Am. Chem. Soc.* **2000**, *122*, 9548.
(8) Khalatur, P. G.; Khokhlov, A. R. *Mol. Phys.* **1998**, *93*, 555.
(9) Khalatur, P. G.; Zherenkova, L. V.; Khokhlov, A. R. *Eur. Phys. J. B* **1998**, *5*, 881.
(10) Gan, H. H.; Eu, B. C. *J. Chem. Phys.* **1998**, *109*, 2011.
(11) Taylor, M. P.; Lipson, J. E. G. *Fluid Phase Equilib.* **1998**, *150*−*151*, 641.
(12) Schweizer, K. S.; Curro, J. G. *Phys. Rev. Lett.* **1987**, *58*, 246.
(13) Curro, J. G.; Schweizer, K. S. *Macromolecules* **1987**, *20*, 1928.
(14) Curro, J. G.; Schweizer, K. S. *J. Chem. Phys.* **1987**, *87*, 1842.
(15) Chandler, D.; Andersen, H. C. *J. Chem. Phys.* **1972**, *57*, 1930.
(16) Chandler, D. in *Studies in Statistical Mechanics VIII*; Montroll, E. W., Lebowitz, J. L., Eds.; North-Holland: Amsterdam, 1982.
(17) Lowden, L. J.; Chandler, D. *J. Chem. Phys.* **1974**, *61*, 5228.
(18) Hansen, J. P.; McDonald, I. R. *Theory of Simple Liquids*; Academic Press: London, 1986.
(19) Yethiraj, A.; Schweizer, K. S. *J. Chem. Phys.* **1993**, *97*, 5927; **1993**, *98*, 9080.
(20) Schweizer, K. S.; Yethiraj, A. *J. Chem. Phys.* **1993**, *98*, 9053.
(21) Weeks, J. D.; Chandler, D.; Andersen, H. C. *J. Chem. Phys.* **1971**, *54*, 5237.
(22) Martin, M.; Siepmann, I. *J. Phys. Chem. B* **1999**, *103*, 4508.
(23) Chandler, D.; Singh, Y.; Richardson, D. M. *J. Chem. Phys.* **1984**, *81*, 1975.
(24) Nichols, A. L.; Chandler, D.; Singh, Y.; Richardson, D. M. *J. Chem. Phys.* **1984**, *81*, 5109.
(25) Pütz, M.; Curro, J. G.; Grest, G. S. *J. Chem. Phys.* **2001**, *114*, 2847.
(26) Curro, J. G.; Schweizer, K. S. *Macromolecules* **1991**, *24*, 6736.
(27) Olabiisi, O.; Simha, R. *Macromolecules* **1975**, *8*, 206.
(28) Beg, S. A.; Tukur, N. M.; Al-Harbi, D. K.; Hamad, E. Z. *J. Chem. Eng. Data* **1995**, *40*, 74.
(29) Narten, A. H. *J. Chem. Phys.* **1968**, *48*, 1630.
(30) Evans, D. J.; Watts, R. O. *Mol. Phys.* **1976**, *32*, 93.
(31) Claessens, M.; Ferrario, M.; Ryackaert, J. P. *Mol. Phys.* **1983**, *50*, 217.
(32) Wick, C. D.; Martin, M. G.; Siepmann, J. I. *J. Phys. Chem. B* **2000**, *104*, 8008.
(33) Honnell, K. G.; McCoy, J. D.; Curro, J. G.; Schweizer, K. S.; Narten, A.; Habenschuss, A. *J. Chem. Phys.* **1991**, *94*, 4659.
(34) Curro, J. G.; Webb, E. B.; III.; Grest, G. S.; Weinhold, J. D.; Pütz, M.; McCoy, J. D. *J. Chem. Phys.* **1999**, *111*, 9073.
(35) Tsige, M.; Curro, J. G.; Grest, G. S.; McCoy, J. D. *Macromolecules* **2003**, *36*, 2158.
(36) Kirkwood, J. G.; Buff, F. P. *J. Chem. Phys.* **1951**, *19*, 774.
(37) Haulait-Pirson, M.; Huys, G.; Vanstraelen, E. *Ind. Eng. Chem. Res.* **1987**, *26*, 447.

MA0355296